UCLouvain

epl

École polytechnique de Louvain

Design, optimisation and fabrication of silicon-based integrated waveguides at millimetre-wave frequencies

Author: **Nicolas Vanpée**
Supervisors: **Dimitri Lederer, Jean-Pierre Rasquin**
Readers: **Isabelle Huynen, Vincent Kaschten**
Academic year 2022 - 2023
Master [120] in Electrical Engineering

Abstract

We live in a world more and more connected where utilization of the hertz wave is part of our daily life. Currently, the main problem with the high frequencies is the size of the waveguide to transmit them.

The purpose of this Master's thesis is to design, optimise, fabricate and measure a substrate-integrated waveguide (SIW) for the W band with a reduced thickness. The material inside the waveguide is a BenzoCycloButene polymer (BCB) which is the main constraint of the design.

Acknowledgements

Firstly, my thanks go to Mr Lederer and Mr Raskin for giving me the opportunity to work on this interesting subject. A special thanks goes to Romain Tuyaerts for the time spent in the laboratory, for always being ready to answer my questions and specifically his thoughts about the fabrication process. Thank you to Lucas Nyssens for his help in analysing my results.

I would like also to thank Sebastien Faniel and Michael Coulombier for their advice given on the different manufacturing processes.

Finally, I would like to express my thanks to my friend Benoît Hermans for proofreading the language.

Contents

Abstract **1**

Acknowledgements **2**

1 Introduction **6**

2 State of the art **8**

2.1 Electromagnetic waves . . . 8

2.1.1 Maxwell's equations . . . 8

2.1.2 W band . . . 9

2.2 Wavesguides . . . 10

2.2.1 Microstrip line . . . 11

2.2.2 Coplanar waveguide . . . 11

2.2.3 Grounded coplanar waveguide . . . 12

2.2.4 Rectangular Waveguides . . . 13

2.2.5 Substrate-integrated waveguide . . . 14

2.2.6 GCPW to SIW transitions . . . 14

2.3 Benzocyclobutene . . . 16

3 Simulations **17**

3.1 Sizing . . . 17

3.1.1 Thickness of the polymer . . . 17

3.1.2 Thickness of the aluminium . . . 19

3.1.3 Width of the waveguide . . . 19

3.1.4 Design of the access . . . 21

3.1.5 Transition . . . 21

3.2 Effects of the fabrication parameters . . . 22

3.2.1 Width of the waveguide . . . 22

3.2.2 Aluminium oxide layer . . . 22

4 Fabrication process **25**
4.1 Manufacturing steps with the photosensitive benzocyclobutene . . . 25
4.2 Manufacturing steps with the non-photosensitive benzocyclobutene 26
4.3 Masks of the design 27
4.4 Choice between the photosensitive and the non-photosensitive . . . 27
4.5 Aluminium deposition by Electron-beam physical vapor deposition . 29
4.6 Plasma cleaning 30
4.7 BCB deposition 30
4.7.1 Adhesion promoter deposition 30
4.7.2 Soft bake for the promoter 30
4.7.3 BCB spin coating 31
4.7.4 Soft bake for the BCB 31
4.7.5 Curing 31
4.8 Lithography 33
4.9 Aluminium etching 35
4.10 BCB etching 35
4.11 Aluminium deposition by sputtering 36
4.12 Lithography cleaning 36
4.13 Final results 37
4.14 Other manufacturing problems 38

5 Measurements **40**
5.1 TRL and mTRL calibration 40
5.2 De-embedding 40
5.3 Results 40
5.4 Discussion 42

6 Conclusion **43**
Proposals for improvement 44

List of Figures **46**

List of Tables **47**

Bibliography **48**

List of Symbols

BCB	BenzoCycloButene
CPW	Coplanar waveguide
CPWG	Coplanar waveguide with ground
GCPW	Grounded coplanar waveguide
HDMS	HexaMethylDiSilazane
SEM	Scanning Electron Microscope
SIW	Substrate Integrated Waveguide
TE	Transverse electric modes
TEM	Transverse electromagnetic modes
TM	Transverse magnetic modes
TRL	Thru-Reflect-Line
Winfab	Wallonia Infrastructure Nano Fabrication

Chapter 1

Introduction

Waveguides are an essential component in many microwave and millimeter-wave systems, used to propagate electromagnetic waves at these high frequencies with minimal loss and high isolation between different channels. The study of waveguides has been a subject of active research for many years, and significant progress has been made in understanding their behavior and performances. In this thesis, a comprehensive study of waveguides is presented, covering the state of the art, simulations, fabrication process, and measurements.

In the second chapter, the first being this introduction, the current state of the art in waveguide research is reviewed. The different types of waveguides and their characteristics are discussed, including the microstrip, coplanar waveguide, GCPW and SIW. Then a transition between GCPW and SIW is described. The BCB characteristics will also be discussed.

In the next chapter, a detailed analysis of waveguide behavior using simulation tools is presented. First, there is a justification of how the waveguide is sized. Then the effects of the variations due to the fabrication are analysed. The results of the simulations for each sizing or fabrication impact are presented.

In chapter four, the process of fabricating waveguide is described. First, there is an explanation of the differences between photosensitive and non-photosensitive BCB. Each step used to manufacture the waveguide is discussed, including photolithography, etching, and deposition. The challenges and limitations of the fabrication process are also discussed, as well as the approaches taken to overcome these challenges.

Finally, the measurement method is explained. The waveguide performances are presented. The impedance of the GCPW line, the measured and de-embedded

propagation constant of the SIW are displayed. And a brief analysis of the results is given.

Chapter 2

State of the art

This chapter presents the different elements needed to well understand the following chapters. The state of the art is divided in four main sections. This begin by introducing what's an electromagnetic wave, its mathematical definition with the Maxwell's equations and the frequency band used. Then the different types of waveguides will be presented. Finally, an explanation on the polymer used in the fabrication is given.

2.1 Electromagnetic waves

2.1.1 Maxwell's equations

Maxwell's equations are a set of four partial differential equations that describe the behavior of electric and magnetic fields. These equations are fundamental to the study of electromagnetism and are among the most important equations in physics.

The first equation, known as Gauss's law for electric fields, states that the flux of the electric field through any closed surface is equal to the charge enclosed within that surface. This equation relates the electric field to the distribution of electric charge in a region.

$$\vec{\nabla} \cdot \vec{E} = \frac{\rho}{\varepsilon_0} \tag{2.1}$$

The second equation, known as Gauss's law for magnetic fields, states that the flux of the magnetic field through any closed surface is always zero. This equation states that the magnetic field is always solenoidal, meaning that it has no sources or sinks.

$$\vec{\nabla} \cdot \vec{B} = 0 \tag{2.2}$$

The third equation, known as Faraday's law of induction, states that the line integral of the electric field around any closed loop is equal to the negative of the time rate of change of the magnetic flux through the loop. This equation describes the relationship between electric and magnetic fields and is the basis for the operation of electric generators and transformers.

$$\vec{\nabla} \wedge \vec{E} = -\frac{\partial \vec{B}}{\partial t} \tag{2.3}$$

The fourth equation, known as the Ampere-Maxwell law, states that the line integral of the magnetic field around any closed loop is equal to the current enclosed within the loop, multiplied by the permeability of free space. This equation relates the magnetic field to the distribution of electric current in a region.

$$\vec{\nabla} \times \vec{B} = \mu_0 \left(\vec{\jmath} + \vec{\jmath}_D \right) \tag{2.4}$$

When applied to waveguides, these equations can be used to analyze the behavior of electromagnetic waves as they propagate through the waveguide. They can be used to predict the characteristics of the waves, such as their frequency, wavelength, and mode of propagation. They can also be used to design and optimize waveguides for specific applications.

2.1.2 W band

The electromagnetic spectrum take all frequencies of the electromagnetic radiations. The lower frequencies with the higher waves length are the radio waves and at the opposite they are the ionizing radiations. Between these two extremes they are the visible light and the microwaves which is the frequency band which interests us.

The microwaves wavelengths ranging from about one meter to one millimeter corresponding to frequencies between 300 MHz and 300 GHz respectively, the W-band is the portion of this electromagnetic spectrum. It falls within the frequency range of 75 - 110 GHz.. The W band is used for a variety of applications, including radar, satellite communication, and wireless networking.

One of the main advantages of the W band is that it has a much higher frequency than lower bands, such as the X band and the C band, which allows for the use of smaller antennas and more compact equipment. This makes it well-suited for use in portable and mobile devices, as well as for applications where size and weight are critical considerations.

However, the W band is also susceptible to atmospheric absorption and scattering, which can limit its range and accuracy in some situations. As a result, it is not

as widely used as some other frequency bands, which have better propagation characteristics.

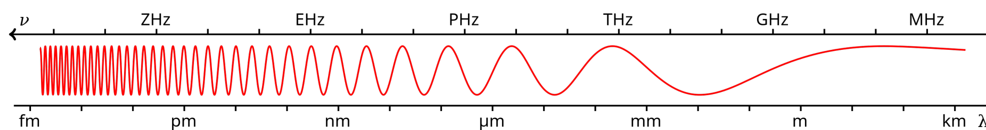

Figure 2.1: Frequency (ν) and wave length (λ).

2.2 Wavesguides

In the W band, waveguides are commonly used to transmit high-frequency electromagnetic waves over long distances with minimal loss of signal strength. They are particularly useful for applications that require high bandwidth and are used in a variety of fields, including telecommunications, radar, and medical imaging.

There are several types of waveguides that can be used in the W band, including metallic waveguides and dielectric waveguides. Metallic waveguides are made of a conductor, such as copper or aluminum, and are used to guide high-frequency signals. They are typically used at higher frequencies and are less lossy than dielectric waveguides. Dielectric waveguides are made of a non-conducting material, such as glass or plastic, and are used to guide lower-frequency signals.

The wave equation is a partial differential equation that describes the behavior of a wave as it propagates through space. In the case of a waveguide, the wave equation can be written as:

$$\nabla^2 E + k^2 E = 0 \tag{2.5}$$

where E is the electric field, ∇^2 is the Laplacian operator, and k is the wave number, which is related to the frequency of the wave.

The boundary conditions for a waveguide describe the behavior of the electric and magnetic fields at the walls of the waveguide. For a waveguide with perfect conducting walls, the boundary conditions can be written as:

$E_x = 0$ and $H_x = 0$

where E_x is the component of the electric field perpendicular to the walls of the waveguide and H_x is the component of the magnetic field perpendicular to the walls.

Using the wave equation and boundary conditions, it is possible to derive the dispersion relation, which describes the relationship between the frequency and

wavelength of the electromagnetic waves that can propagate through the waveguide. The form of the dispersion relation will depend on the shape and dimensions of the waveguide.

Using these equations, it is possible to analyze the behavior of electromagnetic waves in a waveguide and predict how they will propagate through the waveguide. This is useful for designing and optimizing waveguides for specific applications.

In addition to the wave equation and boundary conditions, the behavior of electromagnetic waves in a waveguide can also be described using the modes of propagation. Modes are patterns of electromagnetic energy propagation that are characterized by their frequency, wavelength, and field patterns. The modes of a waveguide are determined by the shape and dimensions of the waveguide and the frequency of the electromagnetic waves. There are several types of modes that can propagate through a waveguide, including transverse electric (TE) modes, transverse magnetic (TM) modes, and hybrid (HE and EH) modes. Each mode has its own unique characteristics and can be used for different applications.

2.2.1 Microstrip line

The microstrip line consists of a strip of conductive material, usually copper or aluminium, which is put on a dielectric material. The conductive strip is the center conductor of the transmission line and the ground plane on the other side of the dielectric is the other conductor. One of the main benefits of a coplanar waveguide is that it can be easily integrated with other components on a single substrate, such as a printed circuit board (PCB). This makes it a popular choice for use in microwave and millimeter-wave circuits. The structure of a microstrip is shown on Figure 2.2. In most case, the thickness (d) is much smaller than the wavelength (λ) and therefore the fields are quasi-TEM. The combination of the substrate and the air can be interpreted as a microstrip line place in a homogeneous effective dielectric. This effective permittivity (ϵ_e) is given by the equation 2.6 with ϵ_r the relative permittivity of the substrate, d the substrate thickness and W the line width.

$$\epsilon_e = \frac{\epsilon_r + 1}{2} + \frac{\epsilon_r - 1}{2} \frac{1}{\sqrt{1 + 12d/W}} \tag{2.6}$$

2.2.2 Coplanar waveguide

The coplanar waveguides (CPW) are similar to the microstrip with the fabrication part, but have a close proximity between the conductor and the ground plane which

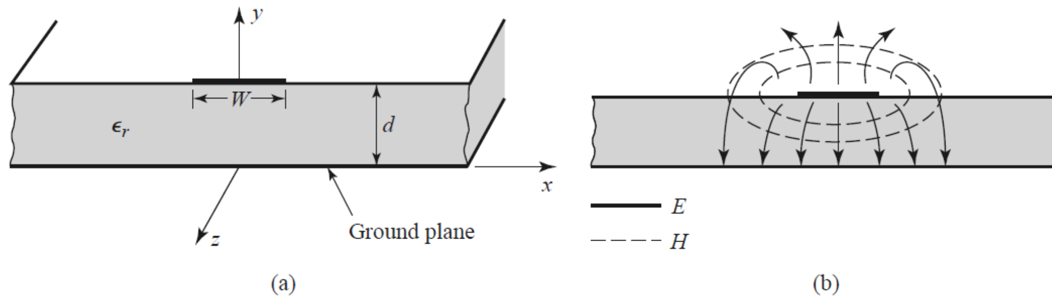

Figure 2.2: Microstrip transmission line. (a) Geometry. (b) Electric and magnetic field lines. [1]

makes it very useful for active circuitry. This disposition give to the geometry multiple advantages : [2]

- High isolation : thanks to the lateral ground, the waveguide has a better isolation.
- Lower loss than striplines : a lower proportion of field lines passes through the dielectric.
- Tunable bandwidth : the distance between the ground and the signal or the width of the signal line can be tuned, the characteristics are modular like the bandwidth.
- Single mode propagation : given that the waveguide is tunable, the cutoff frequency can easily set.

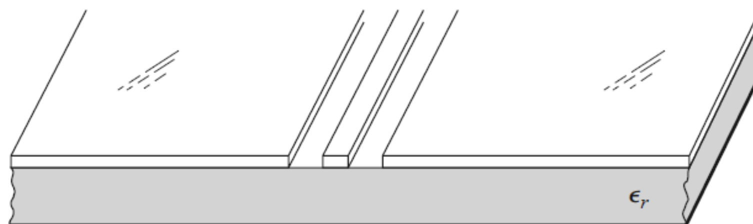

Figure 2.3: Coplanar waveguide geometry. [1]

2.2.3 Grounded coplanar waveguide

Grounded coplanar waveguide is the combination of the microstrip line and the coplanar waveguide. It is composed of a coplanar waveguide with a grounded plane

on the other side of the dielectric. The side ground and the ground plane are connected via metalized walls or holes. Be careful not to be confused with the coplanar waveguide with ground which does not have connection between both sides as shown on Figure 2.4.

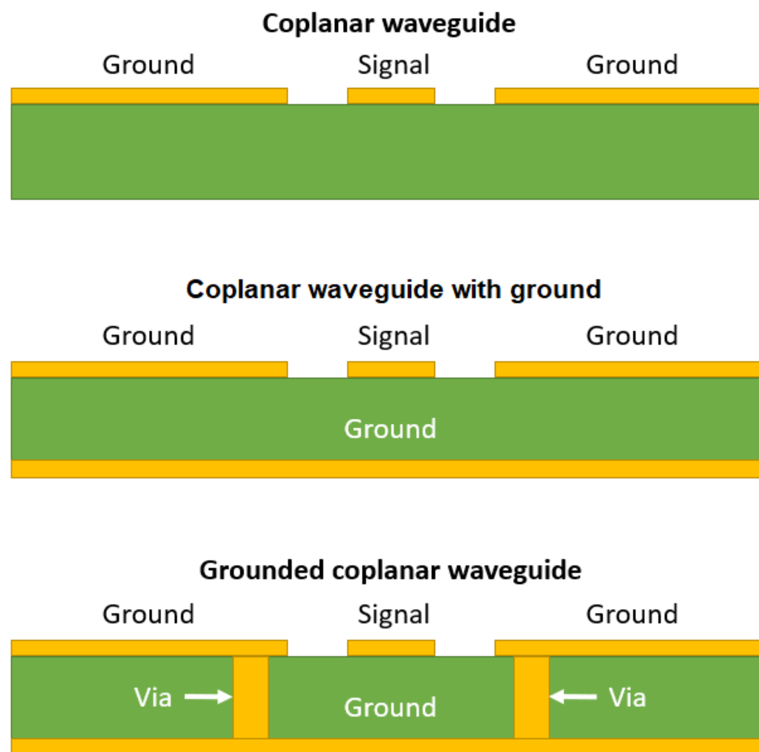

Figure 2.4: Comparison between different type of coplanar waveguide. [3]

2.2.4 Rectangular Waveguides

One of the main advantages of rectangular waveguides is their ability to support a wide range of modes, or patterns of electromagnetic energy propagation. This makes them particularly useful for applications that require high bandwidth and the transmission of large amounts of data. In Figure 2.5, the wave propagation is in the z direction, ϵ and μ are the permittivity and the permeability of dielectric inside the structure. Being composed of only one conductor, the rectangular waveguide can only propagate TM or TE mode. The propagation constant is given by the equation 2.7. [4]

$$\beta = \sqrt{k^2 - (\pi/a)^2} \tag{2.7}$$

with β the propagation constant and k the wave number.

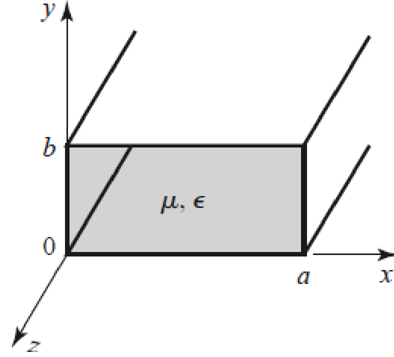

Figure 2.5: Geometry of a rectangular waveguide. [1]

2.2.5 Substrate-integrated waveguide

A substrate-integrated waveguide (SIW) is a type of waveguide that is embedded within a dielectric substrate. It is a relatively new type of waveguide that has gained popularity in recent years due to its compact size, low loss, and high-frequency capabilities. The side walls being composed of vias, the TM mode cannot propagate due to the fact they require a current flow in the direction of propagation. The SIW only propagate TE mode. The width of the waveguide seen by the wave for a well designed structure are equal to the distance between the center of each row of vias. To avoid multiple modes $\lambda_c = 2W$ where W is defined as

$$W = \frac{c_0}{2 \cdot f_c \sqrt{\epsilon_r}} \tag{2.8}$$

with c_0 the speed of light, f_c the cutoff frequency of the mode TE_{10} and ϵ_r the permittivity.

The main rules to design a SIW are : [5]

- $s < d$
- $p/\lambda_c < 0.25$
- $s \leqslant 2 \cdot d$

with s the distance between the center of 2 holes, d the diameter of the holes as presented in Figure 2.6.

2.2.6 GCPW to SIW transitions

A SIW cannot be easily measured, that is why a transition must be done. The waveguide that can be measure in 'Welcome lab' at UCLouvain is the CPW or

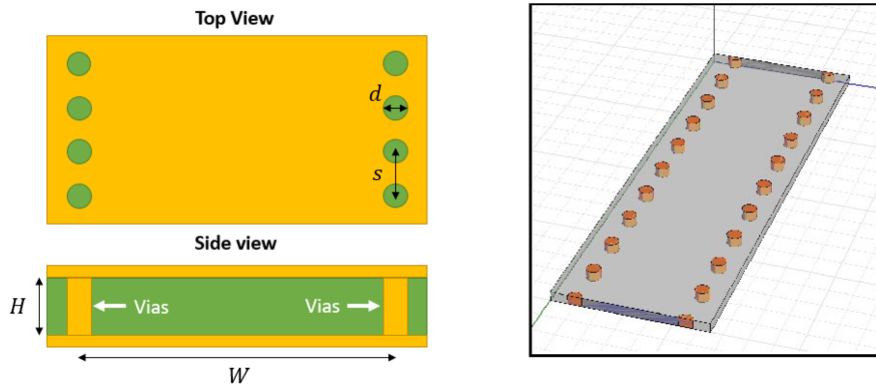

Figure 2.6: Substrate integrated waveguide design and geometry. [3]

GCPW. The transition is a structure that allows electromagnetic waves to be smoothly transferred from one type to the other. The one chosen is the taper. By its gradual change in the geometry, it allows the waveguide mode to evolve smoothly from the GCPW to the SIW. Tapers can be linear or exponential, depending on the required transition length and the desired performance. The exact geometry and the different choices made on it are explained on the Master's thesis by Adam Abazi.

This type is a gradual change in the geometry of the transmission line that allows the electromagnetic wave to move from the GCPW to the SIW or inversely without reflection.

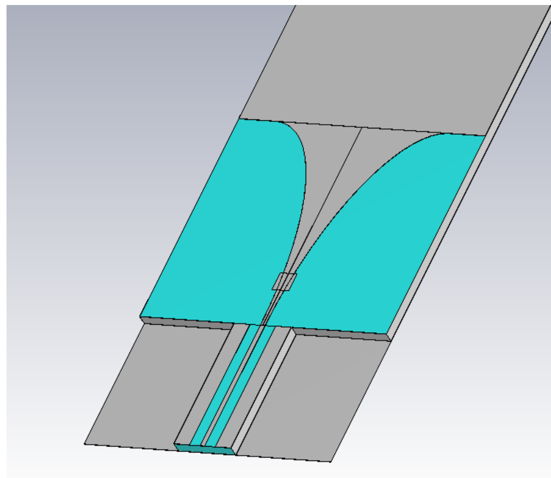

Figure 2.7: Tapered transition without side grounds with capacitive element on BCB substrate-integrated waveguide technology. Grey is metal and blue is the dielectric. The thickness is not to scale. [6]

2.3 Benzocyclobutene

Benzocyclobutene (BCB) is a type of cyclic organic compound with the chemical formula C_8H_8. It is a colorless, crystalline solid that is stable and resistant to thermal and chemical degradation. BCB is widely used as an insulating material in the microelectronics industry, particularly in the production of printed circuit boards (PCBs) and other high-density interconnect devices. One of the main advantages of BCB is its low dielectric constant, which makes it a good choice for use in high-frequency applications where low signal loss is important.

Chapter 3

Simulations

The objective of the simulation is to optimise the dimensions of the devices and see the impact of variations of dimensions due to imperfections of the fabrication process. The dimensions selected for the simulation are :

- Width: $1608\mu m$
- Length: $1200\mu m$
- Thickness of the BCB: $16.5\mu m$
- Thickness of the aluminium: $0.5\mu m$

The simulations are made by varying one parameter at a time.

3.1 Sizing

3.1.1 Thickness of the polymer

Based on two publications ([5] and [7]), a decision was taken to use a thickness around 2 times smaller than that used in these ones. With the polymer available, a final thickness of $16.5\mu m$ has been chosen. The thickness of the polymer is one of the parameter that has the most impact on the waveguide's performances. The finer the thickness, the more it attenuates the signal but at the unlike the others parameters, in this case the attenuation variation is constant for the all W band.

The thinner the layer, the more it attenuates the signal. But, in this case, unlike the other parameters, the attenuation given for a certain thickness is constant inside the W band.

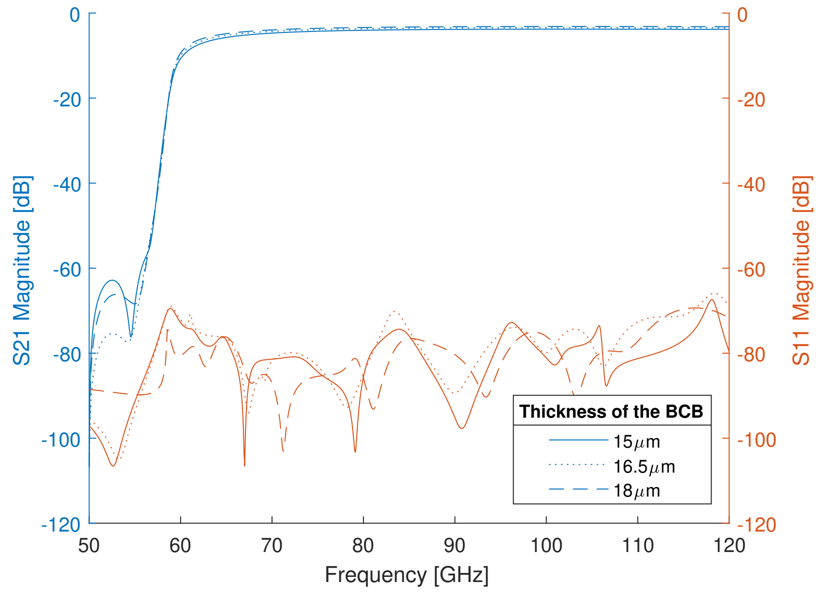

Figure 3.1: S11 and S21 parameters depending on the thickness of the polymer.

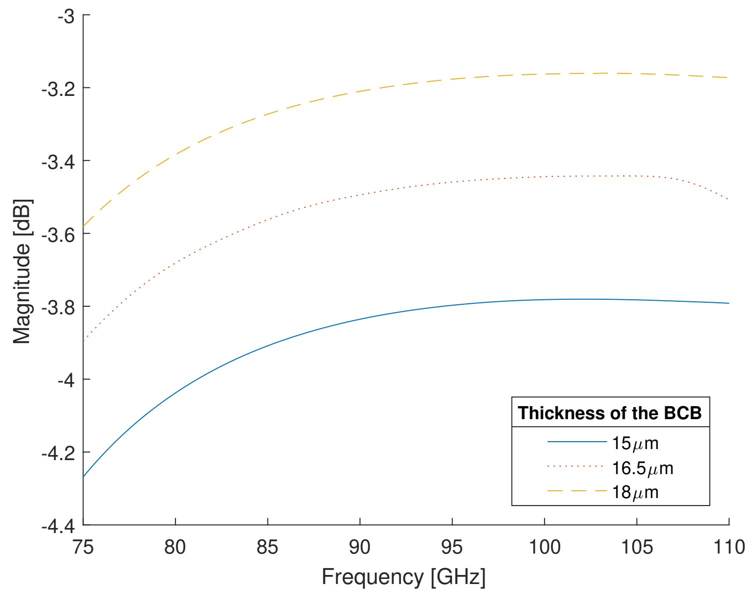

Figure 3.2: Zoom on the W band for S21 parameter depending on the thickness of the polymer.

As show on Figure 3.1, the $S11$ parameter is below $-70dB$ and the cutoff frequency

is the same independently of BCB thickness. At the opposite the $S21$ is proportional in the W band as show on Figure 3.2.

The second impact of the thickness variation is on the access to measure the waveguide. Indeed, as explained later in subsection 3.1.4, the impedance of a GCPW depends on the thickness between the ground and the signal. The more this impedance deviates from the normalised one, the more the reflection between the probes and the GCPW is important.

3.1.2 Thickness of the aluminium

The metal thickness does not have impact given that the transmitted wave is TE, so there is no current in the metal (Figure 3.3). At the opposite, if the transmitted wave was TM, the skin effect should have been taken into account. The skin effect is a phenomenon in which the flow of alternating current tends to distribute itself within a conductor so that the current density is highest at the surface of the conductor and decreases as the depth from the surface increases. The skin depth is given by the equation 3.1.

$$\delta = \sqrt{\frac{2}{\omega\mu\sigma}} = \sqrt{\frac{2\rho}{\omega\mu}} = \frac{1}{\sqrt{\sigma\mu\pi f}} \tag{3.1}$$

- δ : skin depth $[m]$
- ω : angular frequency [rad/s] ($\omega = 2 \cdot \pi \cdot f$)
- f : frequency $[Hz]$
- μ : permeability of the conductor $[H/m]$
- ρ : resistivity of the conductor $[\Omega \cdot m\ ]$ ($\rho = 1/\sigma$)
- σ : conductivity of the conductor $[S/m]$

For the W band, the skin depth is between $0.299nm$ and $0.247nm$.

The choice was therefore determined by the manufacture to have the most optimal aluminium etching result.

3.1.3 Width of the waveguide

The WR10 band works for the frequency between 75 and $110GHz$ and have cutoff frequency of $59GHz$ for the TE_{10} mode. According to the equation 3.2 of the cutoff frequency and the equation 3.3, the width can be calculated.

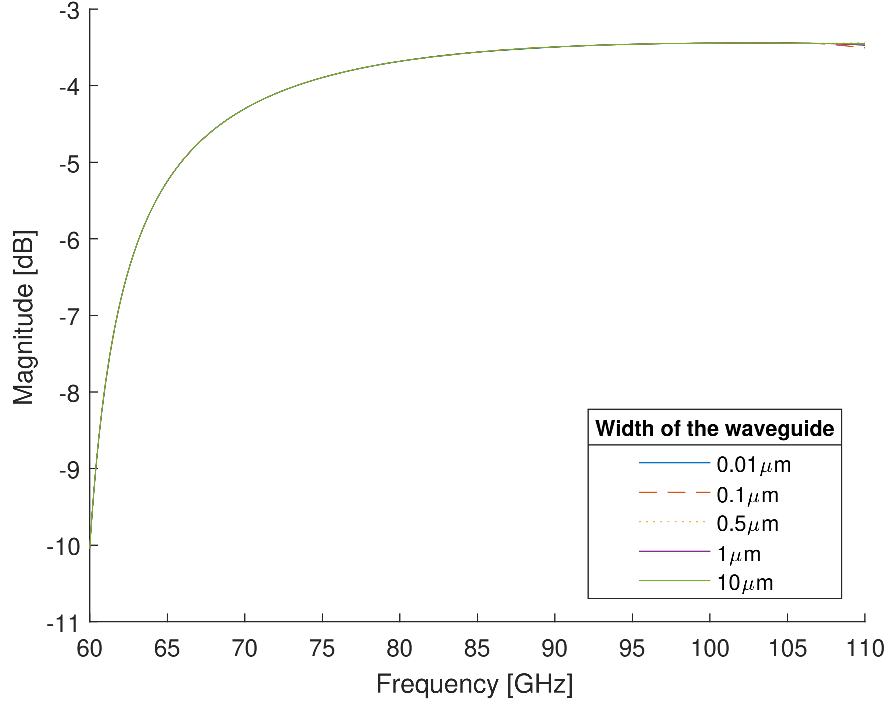

Figure 3.3: S21 parameters depending on the thickness of the metal

$$f_{cmn} = \frac{c_{BCB}}{2\pi}\sqrt{\left(\frac{m\pi}{a}\right)^2 + \left(\frac{n\pi}{b}\right)^2} \tag{3.2}$$

By convention the a corresponds to the largest and b to the smallest dimensions between the height and the width. Knowing that the height is given by the thickness of the substrate and does not work for the desired frequency band, therefore the width is defined by the TE10 mode

$$c_{BCB} = \frac{c}{\sqrt{\epsilon_r}} \tag{3.3}$$

With :

- c_{BCB} : the speed of the electromagnetic wave in BCB
- c : the speed of the electromagnetic wave in the void
- $f_{c10} = 59GHz$
- $\epsilon_r = 2.5$

$$a = \frac{c_{BCB}}{2f_{c10}} \tag{3.4}$$

$$= \frac{\frac{c}{\sqrt{\epsilon_r}}}{2f_{c10}} \tag{3.5}$$

$$= \frac{\frac{3*10^8}{\sqrt{2.5}}}{2*59*10^9} \tag{3.6}$$

$$= 1.608mm \tag{3.7}$$

3.1.4 Design of the access

To measure the waveguide, CPW probes are used. The probes have a defined dimension, to be allowed to measure the SIW, some parameters of the access have to be respected as show on Figure 3.4.

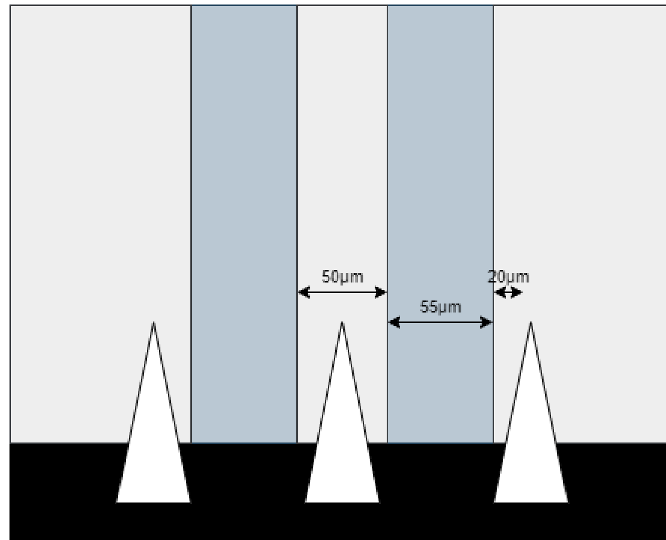

Figure 3.4: Dimension of the GCPW to match requirements of the probe pitch. Light grey represents metal, light blue represents dielectric and white represent the pitch of the probe. [6]

3.1.5 Transition

The transition is the element of the chips which make the link between the SIW and the access. The transition has been design and optimised for the W band by Adam Abazi. Two transition are present on the dies to see the different between the two and were analyzed by Adam.

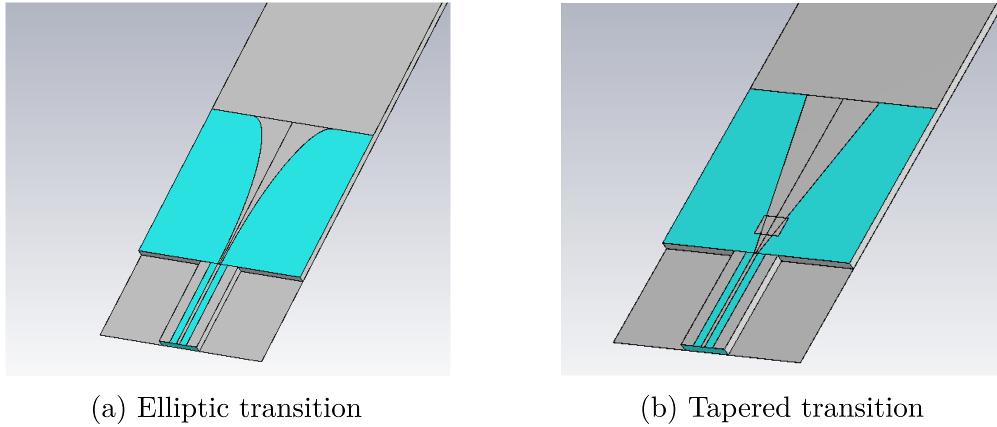

(a) Elliptic transition (b) Tapered transition

Figure 3.5: Transitions on BCB SIW technology. Grey is metal and blue is the dielectric. The thickness is not to scale.

3.2 Effects of the fabrication parameters

3.2.1 Width of the waveguide

As seen in subsection 3.1.3, the width of the waveguide impacts the cutoff frequency but the variations due to fabrication are negligible. The variations come from the variations of aluminum etching with the hard mask and they are below $2\mu m$. As shown in Figure 3.6 with a gap of $50\mu m$, the cutoff frequency are still below $75GHz$ for the first mode and above $110GHz$ for the second mode.

3.2.2 Aluminium oxide layer

After the aluminium deposition when the substrate is removed from the vacuum chamber, due to the oxygen present in the air, a small aluminium oxide layer is formed. This oxide can impact performances by isolating the first layer of aluminum with that deposited after for the side walls. Simulations have been done to see this impact, the Figure 3.7 show that this oxide does not impact significantly the S-parameters in comparison with other parameters like the thickness of the BCB.

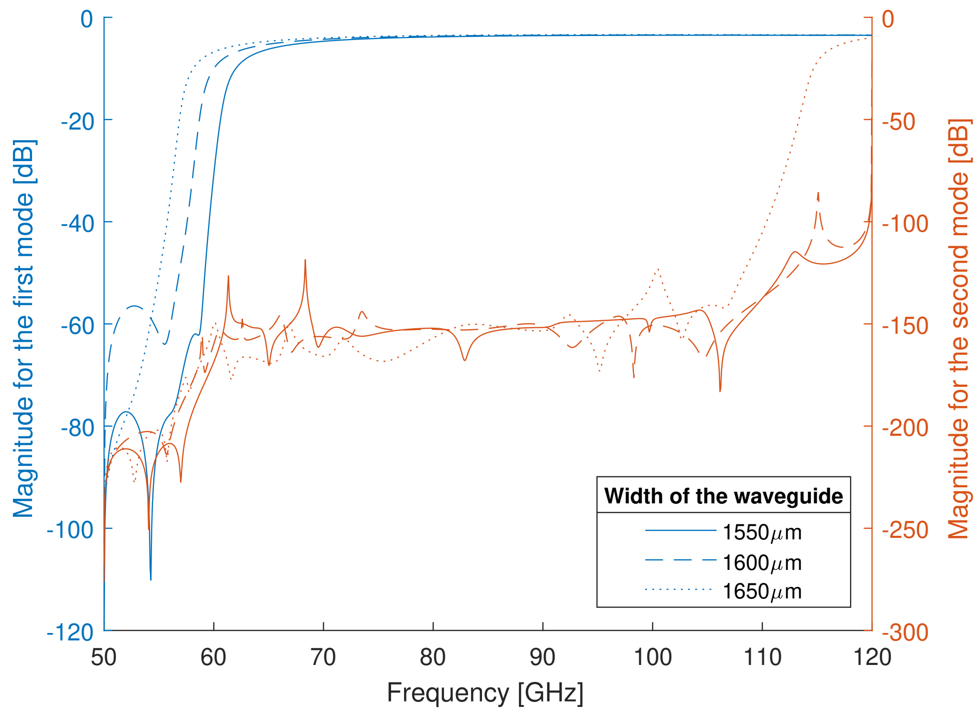

Figure 3.6: S21 parameters depending on the width of the waveguide for the first and second mode.

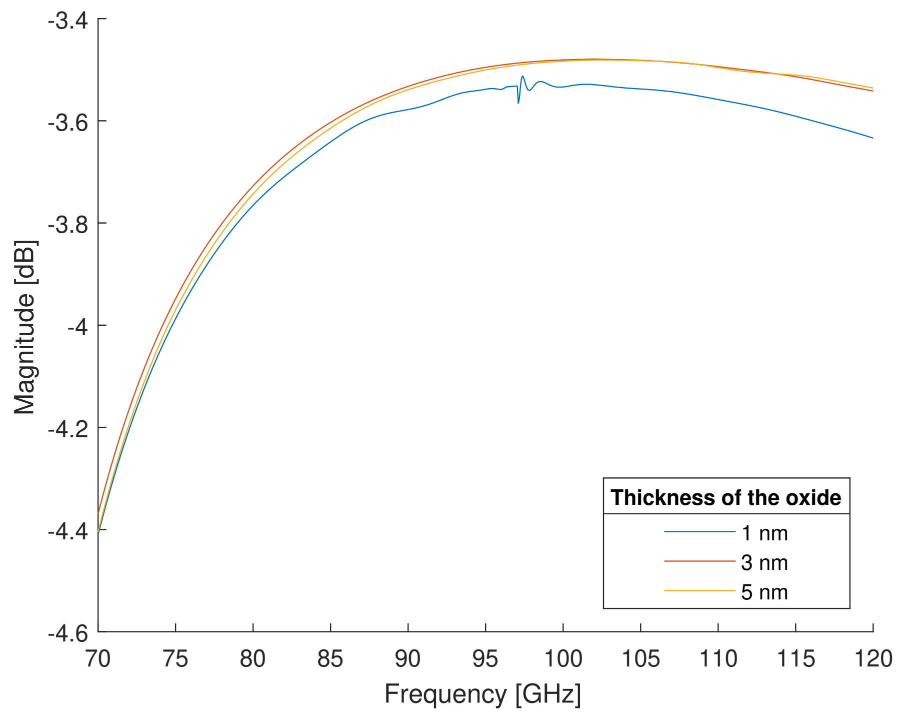

Figure 3.7: S21 parameters depending on the thickness of the oxide.

Chapter 4

Fabrication process

The fabrication process is mainly dependent on the choice of the polymer. For a BCB polymer with the same electrical characteristics, there are two possibilities: photosensitive and non-photosensitive. In the following, both processes allowing to fabricate a SIW are explained but only the second one perform sufficiently during manufacturing to have a working and measurable device. All the manufacturing has been done in the UCLouvain clean room ('Winfab').

4.1 Manufacturing steps with the photosensitive benzocyclobutene

1. Aluminium deposition (see section 4.5)
2. Plasma cleaning (see section 4.6)
3. Benzocyclobutene deposition (see section 4.7) [1]
    (a) Adhesion promoter deposition
    (b) Soft bake
    (c) Spin coating BCB
    (d) Soft bake
    (e) Exposition
    (f) Pre-develop bake

[1] the steps (g), (h) and (j) have been tested in the laboratory with parameters recommended in the datasheet [8], which is why no section is dedicated to them.

(g) Puddle develop

(h) Post-develop bake

(i) Cure

(j) Plasma descum

4. Aluminium deposition by sputtering (see section 4.11)
5. Lithography (see section 4.8)
6. Aluminium etching (see section 4.9)
7. Lithography cleaning (see section 4.12)

4.2 Manufacturing steps with the non-photosensitive benzocyclobutene

1. Aluminium deposition (see section 4.5)
2. Plasma cleaning (see section 4.6)
3. Benzocyclobutene deposition (see section 4.7)
   - Adhesion promoter deposition
   - Soft bake
   - BCB spin coating
   - Soft bake
   - Cure
4. Aluminium deposition (hard mask) (see section 4.5)
5. Lithography (see section 4.8)
   - Photo-resin deposition
   - Spin coating
   - Pre bake
   - Exposition
   - Post exposure bake
   - Development

6. Aluminium etching (see section 4.9)
7. BCB etching (see section 4.10)
8. Aluminium deposition by sputtering (see section 4.11)
9. Lithography (see section 4.8)
10. Aluminium etching (see section 4.9)
11. Lithography cleaning (see section 4.12)

4.3 Masks of the design

To fabricate the complete structure, two masks are needed. The first one (4.4) allows to expose the photosensitive BCB or a negative resin to etch the aluminium and then the BCB. The second one allows to expose a positive resin to etch the final aluminium layer and create the accesses.

The mask is composed of two main elements, dies which contain the different structures and the alignment marks. The alignment marks are different on both masks and they are present to align the two masks perfectly. They are also there to see the lithography and etching quality through lines and holes of different thicknesses.

On each die they are 23 SIW with their accesses and transitions (Figure 4.5). Each SIW is different from the other to have two different transitions, several SIW with different widths and lengths. They are also four GCPW lines (4.4) to be able to de-embed the measurements.

4.4 Choice between the photosensitive and the non-photosensitive

There are many types of BCB and two possibilities are available in the lab with the same electrical properties (Table 4.1). One is photosensitive with a theoretical final thickness between $7.3\mu m$ and $14.2\mu m$. The second one is non-photosensitive but have a theoretical final thickness between $9.64\mu m$ and $26.2\mu m$ [2].

Several tests have been carried out to increase the thickness of the photosensible BCB which would reduce the number of manufacturing steps and therefore the

[2] As explained in subsection 4.7.3, below 1700rpm a dewetting problem present at higher speed increases and no longer allows to have utilisable coated wafer.

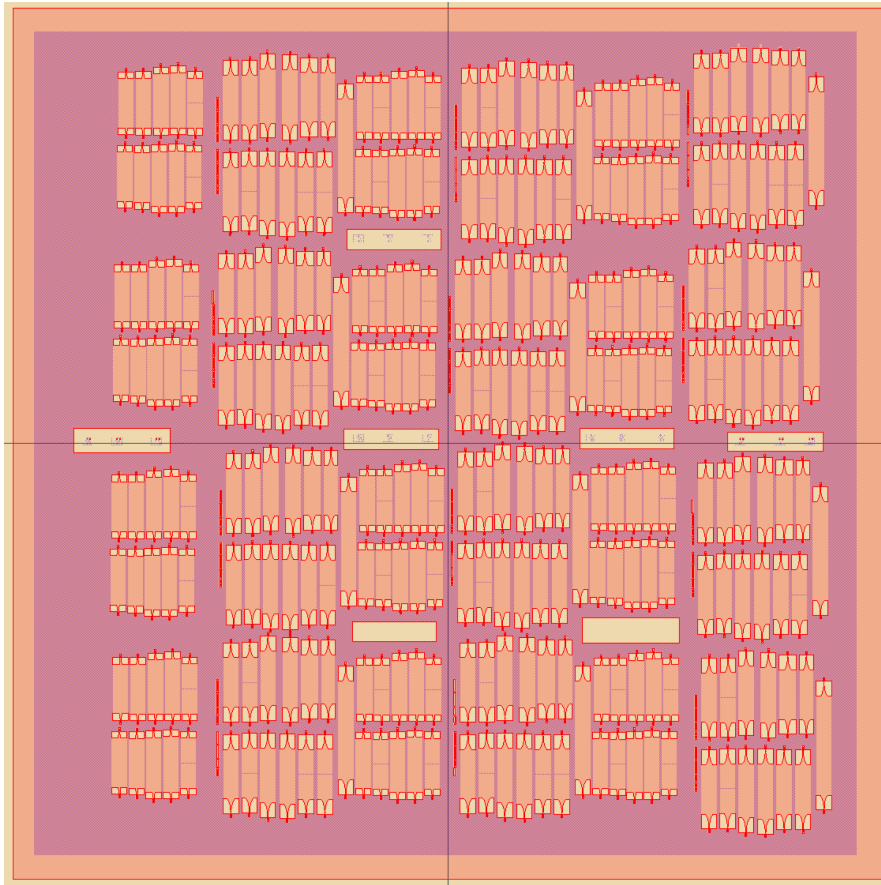

Figure 4.1: First (in blue) and second (in red) masks aligned.

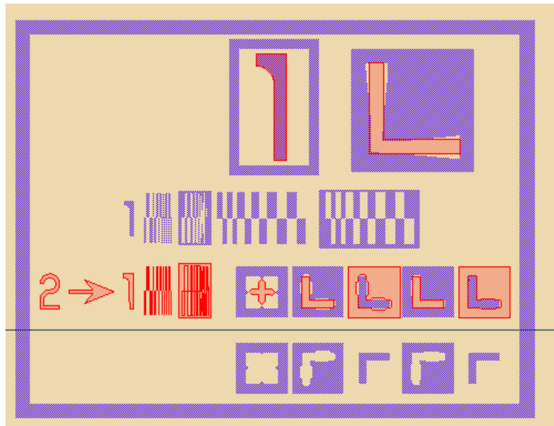

Figure 4.2: Alignment and quality marks.

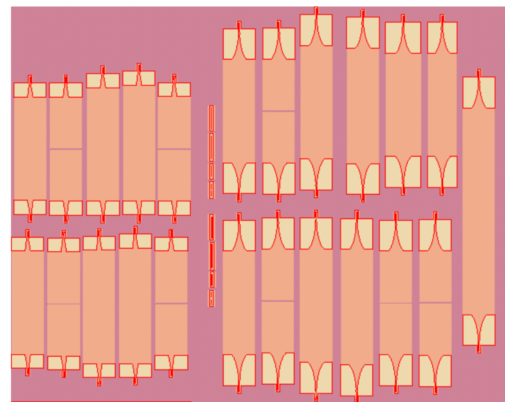

Figure 4.3: Full die.

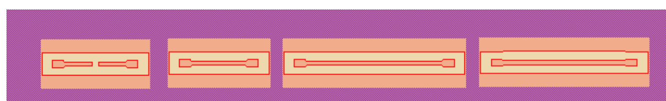

Figure 4.4: GCPW lines.

Figure 4.5: Zoom on a full waveguide.

Property	Measured Value
Dielectric constant	2.65˘2.50 at $1 - 20GHz$
Dissipation Factor	0.0008˘0.002 at $1 - 20GHz$
Breakdown Voltage	$5.3 * 10^6 V/cm$
Volume Resistivity	$1 * 10^{19} \Omega cm$
Thermal Conductivity	$0.29 W/mK$ at 24°C
Leakage Current for BCB3000	$4.7 * 10^{-10} A/cm^2$ at $1.0 MV/cm^2$
Leakage Current for BCB4000	$6.8 * 10^{-10} A/cm^2$ at $1.0 MV/cm^2$

Table 4.1: Electrical and Thermal Properties of BCB (CYCLOTENE 3000 and 4000 resin series).

fabrication process. Unfortunately, none of them gave results. It was therefore finally chosen to manufacture the complete device with the non-photosensitive polymer.

4.5 Aluminium deposition by Electron-beam physical vapor deposition

The first layer and the layer used for the hard mask have to be uniform and are deposited on a flat surface. The easiest method available on lab is the deposition by Electron-beam. The process uses an electron beam to vaporize material from a solid target and deposits it onto a substrate. The electron beam is generated by an electron gun and focused onto the surface of the target material which is placed in a crucible. The high-energy electrons in the beam collide with the atoms in the target, causing them to become excited and vaporized. The vaporized material is then transported to the substrate, where it condenses and forms a thin film.

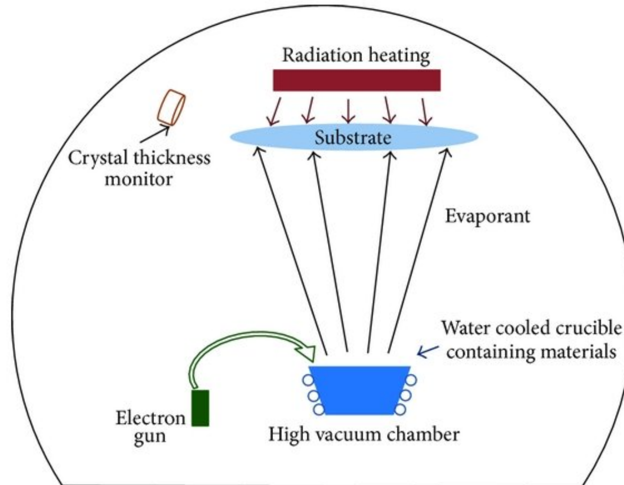

Figure 4.6: Schematic of electron beam evaporation. [9]

4.6 Plasma cleaning

It's important to have a clean surface free of particles or organic contaminants to have a correct adhesion between the metal and the BCB. The cleaning is done thanks to a O_2 plasma.

4.7 BCB deposition

4.7.1 Adhesion promoter deposition

The adhesion promoter for the BCB is different from photo-resist promoter. The HDMS usually used does not work well for the BCB. The promoter used is the AP3000 [10]. The deposition is done thanks to a spin coater. For a wafer of 3.5", $\simeq 2mL$ are deposited in the center. The wafer is rotated at $500rmp$ for $30s$ and then the speed is increased up to $1500rmp$ during $90s$.

4.7.2 Soft bake for the promoter

The goal of the soft bake is to evaporate the solvent present in the liquid. The wafer is placed on a hotplate during $90s$ at $90°C$. Increasing the time does not increase the adhesion of the BCB and, at the opposite, reducing this time leads to a loss of adhesion.

4.7.3 BCB spin coating

The BCB coating is done thanks to a spin coater. For a wafer of 3.5", $\simeq 3mL$ are deposited in the center when rotating at $2rpm$, the speed is increased up to $500rmp$ during $10s$ and finally up to the final speed during $90s$ which depends of the desired thickness.

Spin Speed (RPM)	1000	1500	2000	2500	3000	3500	4000	4500	5000
BCB 3022-63 (μm)	26.2	19.9	16.5	14.4	12.9	11.8	10.9	10.2	9.64
BCB 4026-46 (μm)	/	14.2	11.6	10.2	9.4	8.7	8.1	/	7.3

Table 4.2: Thickness of CYCLOTENE 3022-63 and CYCLOTENE 4026-46 after cure according to the spin speed. [8] [11]

The thicknesses for both BCB below $2500rpm$ was tested and correspond to the datasheet values. But below $1700rpm$ several problems appear. For the non-photosensitive, a dewetting problem, sometimes present at higher speed only at the extremity of the wafer, spreads all over the surface (Figure 4.7). In order to address this problem, the first attempt considered was to add a small layer of gold on the aluminium but this solution did not solve it. The second attempt to have a thicker polymer layer was to deposit two consecutive layers. The dewetting problem also appears during the second deposition. For the photosensitive BCB two other problems are visible after the development, small structures peel off the wafer and for large surfaces, constraints appear in the polymer. These two problem are shown on Figure 4.8.

4.7.4 Soft bake for the BCB

The soft bake for the BCB has the same goal as for the promoter. It is done at $75°C$ during maximum $60s$.

4.7.5 Curing

The polymer must be cure to achieve its final properties and be solid. This curing is done thanks to high temperature without oxygen. For that step, a custom device based on a hotplate and a kitchen saucepan covered by a special lid is used. The lid is equipped by a joint, a manometer to visualize the pressure and a double valve to control the entrance of nitrogen and remove gases. The wafers are placed in the saucepan. Then a lid closes it hermetically thanks to a join. The void is made inside thanks to a pump. After 30s, the nitrogen inlet valve is opened slightly to ensure to replace the remaining oxygen; of course all this while keeping the valve connected to the void pump opened to extract the gases. The pressure inside must

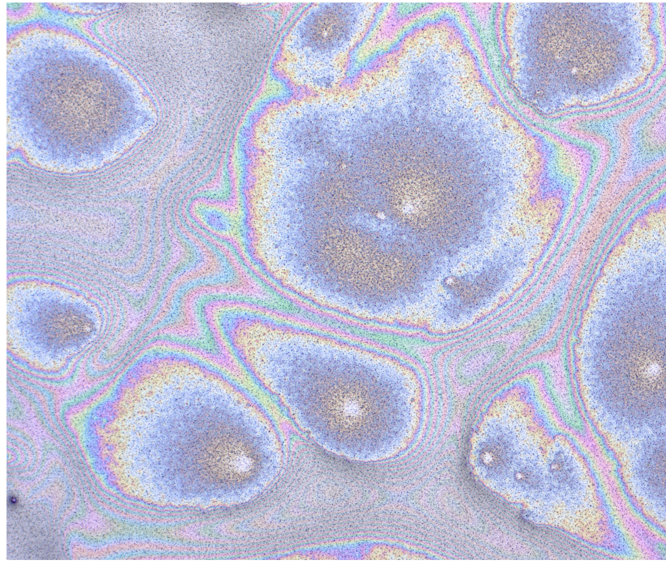

Figure 4.7: BCB dewetting.

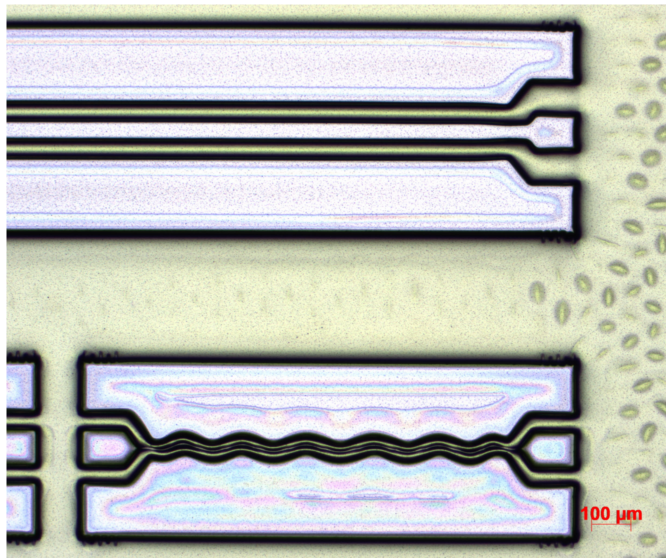

Figure 4.8: Photosensitive BCB after cure with defects.

maintained below the atmospheric pressure to keep the lid airtight. The manometer on the lid allows to check the pressure inside. The Figure 4.9 represents the curing device.

The temperature is increased progressively to reduce the constraints in the polymer. The temperature must never exceed 150°C in presence of oxygen.

- 15 minutes ramp up to 150°C
- 15 minutes kept at 150°C
- 15 minutes ramp up to 250°C
- 60 minutes kept at 250°C
- slow cooling below 150°C

The real temperature in the bottom of the saucepan does not correspond to the set temperature. An offset is present and increases linearly with the temperature. The offsets are given in Table 4.3.

Setpoint temperature [°C]	100	120	140	160	175	180	200	300
Measured temperature without lid [°C]	80	100	120	132		148	165	240
Measured temperature with lid [°C]					150			270

Table 4.3: Measured temperatures on the bottom of the saucepan.

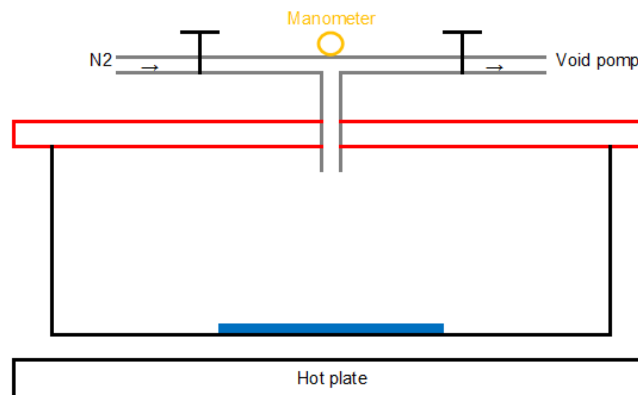

Figure 4.9: Scheme of the curing device. Wafer in blue, lid in red and saucepan in black.

4.8 Lithography

The principle of lithography is to expose a light-sensitive resin to UV light. In the process two different resins are used - a positive one where the light-exposed part becomes soluble in the developer and the unexposed photoresist part remains insoluble. A negative one reacts in the opposite way. The positive resins usually give better results, that is why a positive mask is used for the second. The first

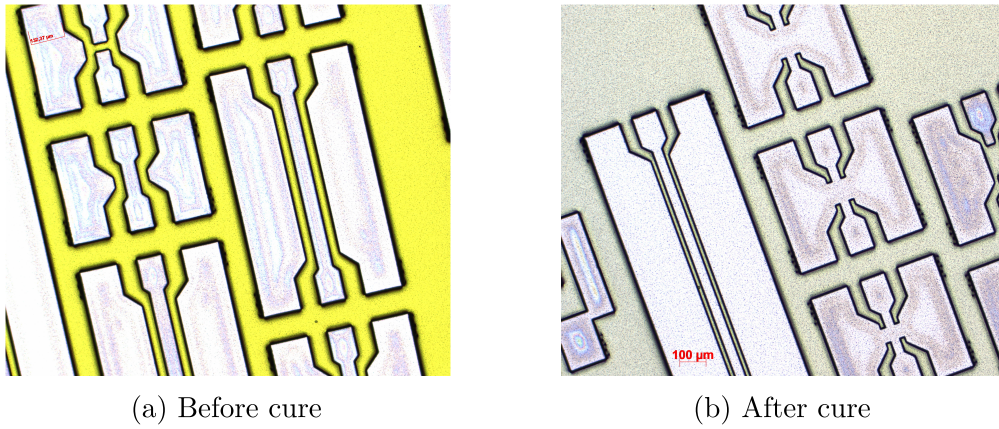

(a) Before cure (b) After cure

Figure 4.10: Test structures with photosensitive BCB.

one being, designed to be used with the photosensitive BCB, is negative as the polymer. The process is similar to all resins, only the power and the time of exposure differ. Unlike some resins overexpose the photo-BCB is not a problem and give equivalent results. The optimal power directly depends of the thickness and is equal to $60mJ/cm^2$ per μm.

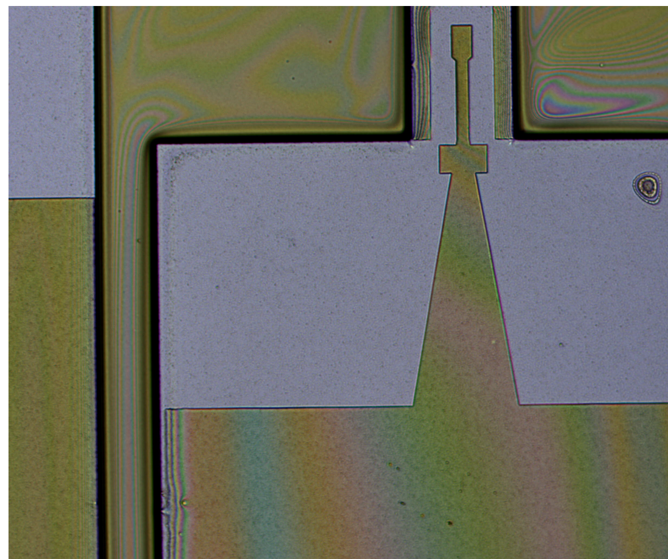

Figure 4.11: Lithography on the aluminium layer (step 9 of the non-photosensitive process).

4.9 Aluminium etching

The aluminium etching is a wet etching. The wafer is immersed in a H_3PO_4 bath heated at $70°C$. The reaction releases gas in the form of small bubbles which appear on the surface. The etching rate strongly depends on the temperature that is why it is important to look when the bubbles quantity decreases to take back the wafer from the solution to stop the reaction and avoid over-etching.

4.10 BCB etching

The BCB has to be plasma etched. The plasma required oxygen and fluorine species to etch the BCB. Several gases are proposed in the datasheet of the BCB. The etch speed depends of several parameters :

- Type of fluorine-containing gas (CF_4, C_2F_6, C_4F_8, SF_6, NF_3, etc.)
- Percentage between oxygen and fluorine-containing gas
- Flow of the gases
- Power of the plasma
- Pressure in the chamber

Oxygen plasma without a fluorine component can create an undesirable amorphous silicon oxide on the surface, thus, the etching process becomes self-passivating and the etch rate slows down and eventually stops.[11]

Depending on the gases available in the cleanroom and the performances of each, a combination of oxygen (O_2 and sulphur hexafluoride (SF_6) has been chosen. To optimise the etch speed, several gas ratios have been tested. The best etching rate was obtained with an equal proportion between the two. The other parameters like the power, the temperature and the pressure are kept constant and are given in Table 4.4. With those parameters, a duration between 22 and 24 minutes is required to etch $16.5\mu m$. The equipment used is the Oxford Plasmalab 100. It is equipped with a ICP-RIE chamber.

Parameters	SF_6 flow	O_2 flow	Pressure	Temperature	ICP power	RF power
Value	$80SCCM$	$80SCCM$	$10Torr$	15°C	$1500W$	$65W$

Table 4.4: Parameters of the Oxford Plasmalab 100 for BCB etching.

It is important to etch the entire thickness in just one time to avoid steps in the polymer as shown on Figure 4.12b.

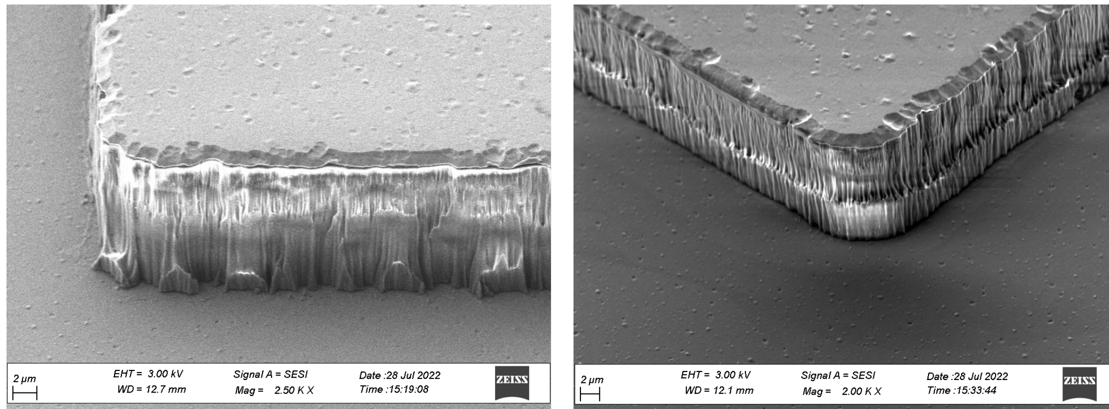

(a) Uniform etching done in one step (b) Non-uniform etching done in two steps

Figure 4.12: Etched BCB taken with SEM (step 7 of the non-photosensitive process).

4.11 Aluminium deposition by sputtering

For the final layer, the aluminium must also be deposited on the wall of the SIW. Therefore, the electron beam evaporation can not be used. The selected method is the sputtering which is a type of physical vapor deposition. A solid target material is bombarded with energetic particles, such as ions, so that atoms of the target material are ejected and deposited onto the substrate. The process can be used to deposit a wide range of materials, including metals, semiconductors, and insulators. In our case, the solid target is aluminium. The aluminium atoms collide with the ions present in the chamber resulting in an indirect deposition on the wafer. To improve the uniformity of the deposit, the target and the wafer are not aligned and the wafer is in rotation.

The aluminum layer deposited is $500nm$. The sputtering result on the BCB is shown on Figure 4.13.

4.12 Lithography cleaning

After the wet etching of the aluminum to create the accesses and the transitions, the complete design is finished. To be able to measure the SIW and have a good contact between the probes and the aluminium, the resin must be removed. The cleaning is done with acetone and rinsed with deionized water.

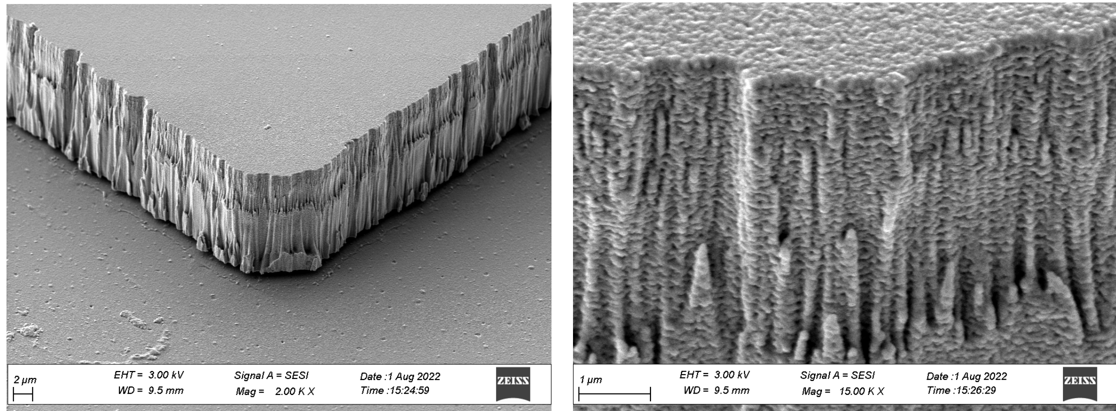

(a) Sides and ground of the SIW (b) Zoom on the upper part of the side

Figure 4.13: Final layer of aluminium sputtered on the top and sides of the SIW taken with SEM (step 8 of the non-photosensitive process).

4.13 Final results

After the final stage and before the electromagnetic measurements, the wafer was analysed to check whether the final dimensions correspond to those expected. The first measurement was made with the profilometer and can be seen on Figure 4.14. The BCB thickness is around $16.5\mu m$. The walls are perfectly vertical. The thickness of the aluminium line above the BCB (access line) is equal to $1\mu m$ which corresponds to the double of $500nm$ layer deposited, one for the hard mask and the second one for the side walls.

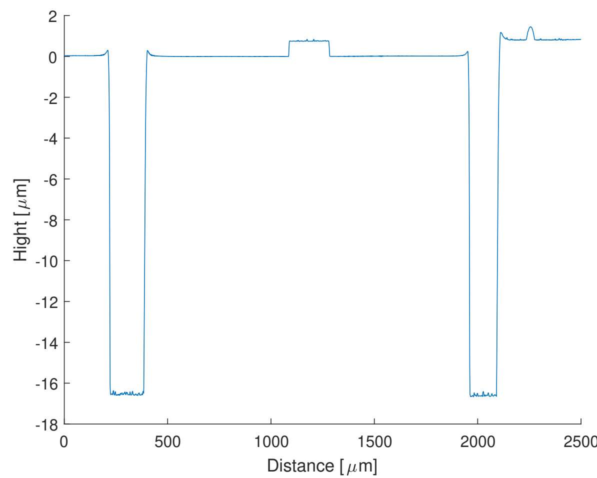

Figure 4.14: Profilometer results for the SIW access.

The second measurement was made using the SEM and gave the Figure 4.13, this measurement allows to check that the aluminum is uniformly deposited on the side walls and well connected with the ground plane.

The third is made under a microscope to check the upper surface and examine the quality of the last aluminium etching and the absence of photoresin (see Figure 4.15). This also allows to check the general quality of the lithography and etching by examining the quality marks.

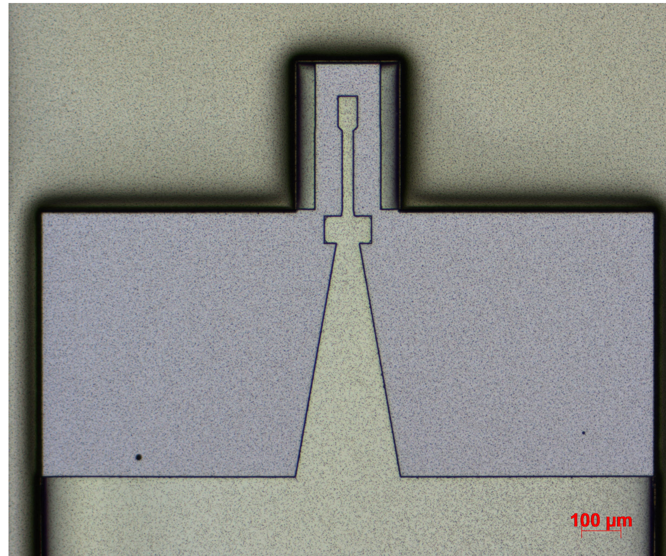

Figure 4.15: Microscope image of an access and a transition.

4.14 Other manufacturing problems

Other problems may arise during manufacturing. One of the most common is the appearance of bubbles. Small bubbles can be trapped in the BCB due to its viscosity during handling (syringes filling used to deposit the BCB on the wafer). During the spin coating, these bubbles make imperfections on the surface . The Figure 4.16 shows the thickness variations. A solution to avoid this problem is to prepare in advance the syringes and handle the BCB carefully.

Another imperfection may appear during the aluminium etching step. If the wafer is left too long in the solution, an important under etching appears (see Figure 4.17) which has a big impact on the impedance of the access and of the transition .

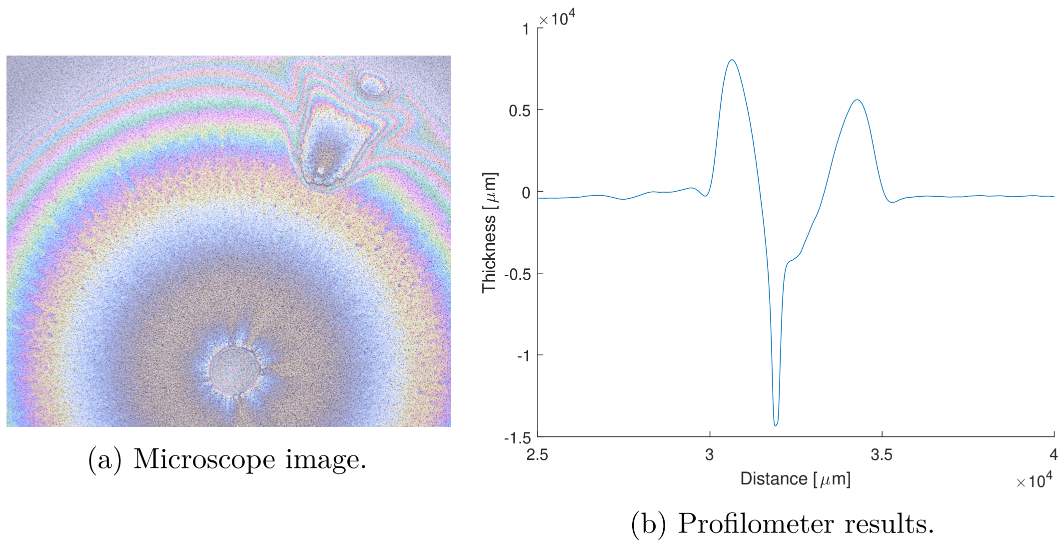

(a) Microscope image.

(b) Profilometer results.

Figure 4.16: Bubble in BCB.

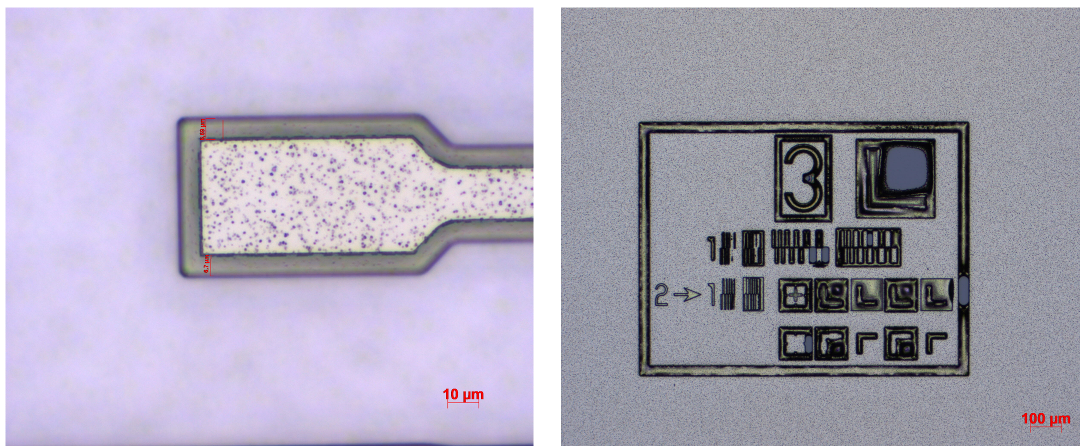

Figure 4.17: Over-etching of $6.7\mu m$ on the access.

Figure 4.18: Alignment and quality marks at the end of the process.

Chapter 5

Measurements

5.1 TRL and mTRL calibration

The TRL calibration is a method used to have the impedance, to calibrate the transmission and reflection characteristics of a device. It can also be used for de-embedding S-parameter data. This method is based on the measurement of a three different lines: a thru, an open (or a short) and a line.

To have a better characterisation and be able to shift the reference plane for the de-embedding the mTRL is used. The mTRL is the 'multi-line Thru-Reflect-Line'. It uses at least two or more lines, in addition with the thru and the open, to make the calibration. More lines there are, more accurate the calibrations will be.

5.2 De-embedding

The first calibration is done on the GCPW lines, on each die they are four GCPW lines, a Thru, an open and two lines. Using a script written by Lucas Nysten and the measurements, an estimation of the propagation constant is calculated (Figure 5.1). To ignore the GCPW lines in the SIW measurements, the estimated constant has to be substract from the results.

5.3 Results

The measurements have been made with the Prober MPI 300nm which is a semi-Automated Probe System of the 'Welcome lab' able to measure a frequency up to 110GHz. The problem with this device is that the measurements are destructive

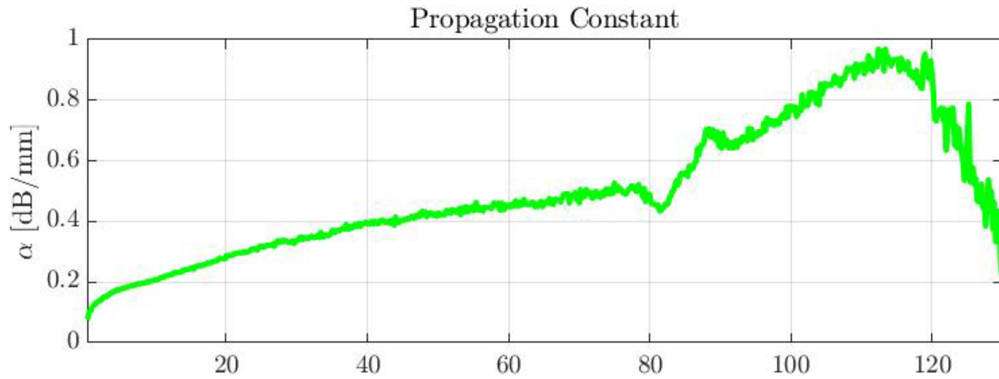

Figure 5.1: Estimation of the propagation constant of the GCPW lines.

for the accesses as shown on Figure 5.4 where two measurements have been done.

The first interesting element to look at is the impedance of the GCPW which is strongly above the normalized impedance of 50Ω due to over-etching.

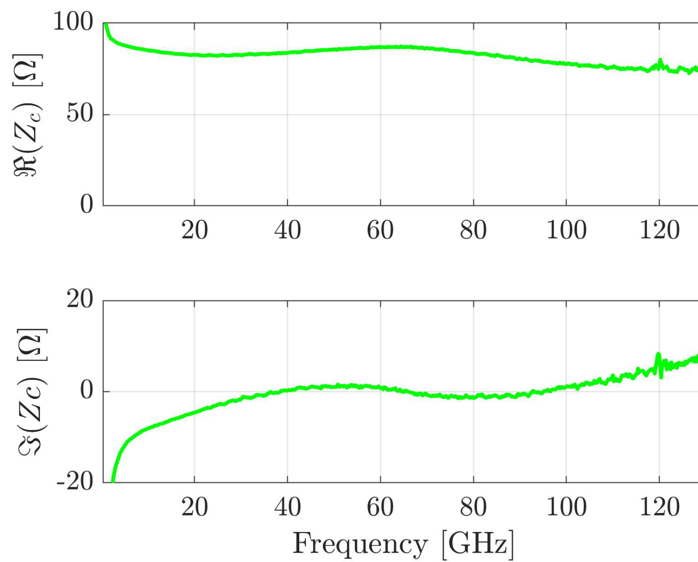

Figure 5.2: Measured impedance of the GCPW lines.

The Figure 5.3 gives the propagation constant (α) for two SIW with different widths. This parameter should impact the cutoff frequency but, due to the impedance mismatch and transition imperfections, both results are similar.

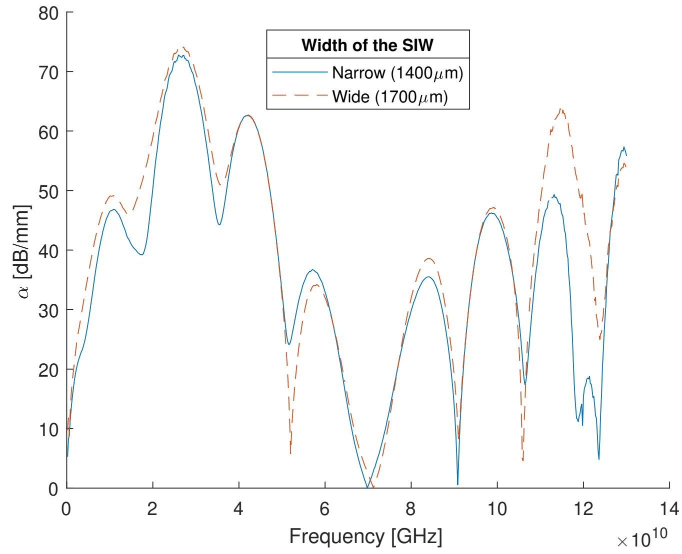

Figure 5.3: Measured and de-embedded propagation constant of the SIW.

5.4 Discussion

Due to an over-etching on the measured wafer, the impedance of the probes were not matched with the GCPW line. Therefore an important part of the signal was reflected. This problem, combined with transition and access imperfections, engenders that the results analysis do not give interesting data.

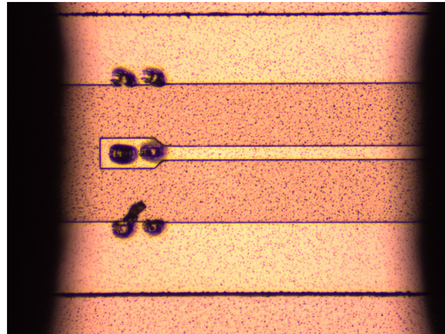

Figure 5.4: Degradation of the access due to the measurements.

Chapter 6

Conclusion

The objective of this thesis was to be based on an already existing SIW design with the aim of reducing its thickness by two while maintaining the same properties. On the basis of two publications ([5] [7]), a reflection on the modification of the parameters that have a weak or strong impact on the final performance of the device was carried out.

Simulations were then run to see the impact of these different parameters and to adapt them to this new thickness constraint.

Those simulations showed that thickness of the BCB and the width of the accesses and transitions are the two main important parameters of the design. At the opposite, a presence of aluminium oxide or the thickness of the aluminium does not change the performance of the SIW.

The fabrication process has been the longest and the most difficult part of this work. Indeed the use of the BCB in 'Winfab' was a first. All elements like deposition, adhesion, cure and etching of the polymer were to be learned. A lot of solutions have been tested to improve the processes to be able to manufacture the final device, sometimes successfully, sometimes without improvement.

Finally, electromagnetic measurements were made to analysed the final specifications of the device. The results given revealed the general SIW performances. This provided to Adam Abazi enough data to demonstrate that the trend in the simulated transitions was well reflected in the measurements. But unfortunately, due to variations in manufacturing such as over-etching and differences between the perfect world of the simulation and the reality, the measurements did not allow to verify the impact of some parameters on the final specifications.

Proposals for improvement

For further research, several elements can be optimized to improve the manufacturing process.

- Try different methods to successfully increase the BCB thickness as the temperature of the pre bake adhesion promoter.
- Vary the plasma power or the pressure during etching to reduce the time of this step and have walls as smooth as possible.
- Measure the etch rate of the aluminium in the H_3PO_4 depending on the temperature of the liquid to avoid over or under-etching.
- Increase the thickness of the top aluminium layer to reduce and avoid peeling of this layer during the measurements

List of Figures

2.1 Frequency (ν) and wave length (λ). 10
2.2 Microstrip transmission line. (a) Geometry. (b) Electric and magnetic field lines. [1] 12
2.3 Coplanar waveguide geometry. [1] 12
2.4 Comparison between different type of coplanar waveguide. [3] . . . 13
2.5 Geometry of a rectangular waveguide. [1] 14
2.6 Substrate integrated waveguide design and geometry. [3] 15
2.7 Tapered transition without side grounds with capacitive element on BCB substrate-integrated waveguide technology. Grey is metal and blue is the dielectric. The thickness is not to scale. [6] 15

3.1 S11 and S21 parameters depending on the thickness of the polymer. 18
3.2 Zoom on the W band for S21 parameter depending on the thickness of the polymer. 18
3.3 S21 parameters depending on the thickness of the metal 20
3.4 Dimension of the GCPW to match requirements of the probe pitch. Light grey represents metal, light blue represents dielectric and white represent the pitch of the probe. [6] 21
3.5 Transitions on BCB SIW technology. Grey is metal and blue is the dielectric. The thickness is not to scale. 22
3.6 S21 parameters depending on the width of the waveguide for the first and second mode. 23
3.7 S21 parameters depending on the thickness of the oxide. 24

4.1 First (in blue) and second (in red) masks aligned. 28
4.2 Alignment and quality marks. 28
4.3 Full die. 28
4.4 GCPW lines. 29
4.5 Zoom on a full waveguide. 29
4.6 Schematic of electron beam evaporation. [9] 30
4.7 BCB dewetting. 32

4.8 Photosensitive BCB after cure with defects. 32
4.9 Scheme of the curing device. Wafer in blue, lid in red and saucepan in black. 33
4.10 Test structures with photosensitive BCB. 34
4.11 Lithography on the aluminium layer (step 9 of the non-photosensitive process). 34
4.12 Etched BCB taken with SEM (step 7 of the non-photosensitive process). 36
4.13 Final layer of aluminium sputtered on the top and sides of the SIW taken with SEM (step 8 of the non-photosensitive process). 37
4.14 Profilometer results for the SIW access. 37
4.15 Microscope image of an access and a transition. 38
4.16 Bubble in BCB. 39
4.17 Over-etching of $6.7\mu m$ on the access. 39
4.18 Alignment and quality marks at the end of the process. 39

5.1 Estimation of the propagation constant of the GCPW lines. 41
5.2 Measured impedance of the GCPW lines. 41
5.3 Measured and de-embedded propagation constant of the SIW. . . . 42
5.4 Degradation of the access due to the measurements. 42

List of Tables

4.1 Electrical and Thermal Properties of BCB (CYCLOTENE 3000 and 4000 resin series). 29
4.2 Thickness of CYCLOTENE 3022-63 and CYCLOTENE 4026-46 after cure according to the spin speed. [8] [11] 31
4.3 Measured temperatures on the bottom of the saucepan. 33
4.4 Parameters of the Oxford Plasmalab 100 for BCB etching. 35

Bibliography

[1] D. M. Pozar, *Microwave Engineering, 4th Edition.* John Wiley & Sons, 2011.

[2] Z. Peterson, "Coplanar waveguide design for your rf pcb." https://www.nwengineeringllc.com/article/coplanar-waveguide-design-for-your-rf-pcb.phpm. Accessed: 2023-01-02.

[3] Z. Peterson, "Substrate integrated waveguide design for rf pcbs." https://www.nwengineeringllc.com/article/substrate-integrated-waveguide-design-for-rf-pcbs.php. Accessed: 2023-01-02.

[4] M. Moulin, "Design and optimization of passive circuits in a polymer technology for sub-thz applications," Master's thesis, Université Grenoble Alpes, 2019-2020.

[5] G.Acri, E.Pistono, F.Podevin, P.Ferrari, L.Boccia, A.-S. Grimault-Jacquin, N. Zerounian, F. Aniel, and L.Vincent, "Benzocyclobutene-based in-package substrate integrated waveguides for sub-thz applications,"

[6] A. Abazi, "Design, fabrication and testing of wideband grounded coplanar waveguide (gcpw) to substrate-integrated waveguide (siw) transitions for w band circuits," Master's thesis, UCLouvain, August 2022.

[7] G.Acri, E.Pistono, F.Podevin, P.Ferrari, L.Boccia, A.-S. Grimault-Jacquin, N. Zerounian, F. Aniel, and L.Vincent, "Guides d'onde siw sur interposeur polymère pour applications millimétriques,"

[8] The Dow Chemical Company, *CYCLOTENE* 4000 Series Advanced Electronic Resins (Photo BCB)*, March 2009.

[9] S. Ahmadi, N. Asim, M. Alghoul, F. Hammadi, K. Saeedfar, N. Ludin, S. Zaidi, and K. Sopian, "The role of physical techniques on the preparation of pho-

toanodes for dye sensitized solar cells," *International Journal of Photoenergy*, vol. Volume 2014, p. 19, 02 2014.

[10] The Dow Chemical Company, *Adhesion Promoter AP3000*, July 2006.

[11] The Dow Chemical Company, *CYCLOTENE* 3000 Series Advanced Electronic Resins*, February 2005.

UNIVERSITÉ CATHOLIQUE DE LOUVAIN
École polytechnique de Louvain
Rue Archimède, 1 bte L6.11.01, 1348 Louvain-la-Neuve, Belgique | **www.uclouvain.be/epl**